Journal of Volcanology and Geothermal Research 180 (2009) 277–291

Contents lists available at ScienceDirect

Journal of Volcanology and Geothermal Research

journal homepage: www.elsevier.com/locate/jvolgeores

Growth and evolution of an emergent tuff cone: Considerations from structural geology, geomorphology and facies analysis of São Roque volcano, São Miguel (Azores)

Vittorio Zanon *, José Pacheco, Adriano Pimentel

Centro de Vulcanologia e Avaliação de Riscos Geológicos, Universidade dos Açores, Rua Mãe de Deus, 9501-801 Ponta Delgada, Portugal

ARTICLE INFO

Available online 10 October 2008

Keywords:
tuff cones
morphological changes
tectonic
facies analysis
Azores

ABSTRACT

The syn-eruptive and post-eruptive history of São Roque tuff cone, its geological setting and volcanological features were studied in detail to understand the role played by the different factors that contributed to the morphological evolution of this relatively simple and small volcanic edifice.
In addition, attention was also focused on the series of natural changes that affected the tuff cone during the course of the years and that finally led to its structural disassembly. A novel model is proposed to explain this process.
The São Roque volcanic centre, located on the island of São Miguel (Azores), consists of two well-consolidated bodies and numerous small islets that formed more than 4700 years ago during the hydromagmatic activity that took place along an intruding dyke, whose NNW–SSE trend is in agreement with the regional tectonic pattern. The eruptive vents probably migrated progressively from SSE to NNW, forming small edifices through the rapid accumulation of sediments during alternating phases of "dry" and "wet" magmatic emissions. Syn-eruptive partial collapses greatly modified the original morphological structure of these edifices, probably allowing sea water to continuously flow into the vents. The complex interaction of these factors controlled the depth of magma fragmentation, producing different types of deposits, in which the ash-lapilli ratio varies considerably. The high-water saturation degree of these deposits caused syn-eruptive and post-eruptive remobilization which resulted in collapses and some small-scale landslides.
Post-eruptive, WNW–ESE trending transtensional and extensional tectonic activities operated during the initial dissection of the cone, generating instability. Furthermore, the rapid accumulation of "wet" tephra, and its following consolidation, caused selective collapses that favoured the fragmentation of the deposit and caused the formation of numerous islets separated by radially-arranged channels. Collapses also involved the lava units emplaced in more recent times around the tuff cone, which show that brittle deformation has been significant in the area for a prolonged period.

© 2008 Elsevier B.V. All rights reserved.

1. Introduction

Landforms created by the accumulation of volcanic material around a vent include a wide range of morphological structures, mainly related to the eruption style and to the physico-chemical parameters of ascending magma (Thouret, 1999), but also depending on the geometry of the feeding dyke and on the pre-existing relief. During a single eruptive event, there may be considerable changes in the eruption style due to changes in the volume and velocity of ascending magma in the feeder dyke (Houghton and Hackett, 1984; Houghton and Schmincke, 1986; Houghton et al., 1999). Additionally, the influence of numerous other factors, such as type, level, and lithology of aquifers, resistance of country rocks, ground-water characteristics may affect the eruptions style (Sohn, 1996; White, 1996). The active stress-field of the area is a crucial factor controlling the rise of magma through the crust (Zanon, 2005), and therefore is a major influence on eruptions magnitude and intensity, controlling the rise of magma batches through the crust, leading to their eruption.

The complex dynamics of water-magma interaction determines the nature of explosive activity, characterized by variable energy outputs and different degrees of magmatic or hydromagmatic fragmentation (Wohletz and Sheridan, 1983; Houghton and Hackett, 1984; Kokelaar, 1986; White and Houghton, 2000; Mastin et al., 2004). Depending on the extent of water-magma interaction, deposits can be formed by fallout layers made of couplets of ash and lapilli, by the alternation of fallout layers and surge deposits, or by the simultaneous concurrent deposition from both processes, leading to the formation of highly complex deposits made of numerous (from few tens to over thousands) of thin tephra beds (e.g. Cas and Wright, 1987; Sohn and Chough, 1989; Dellino and La Volpe, 1995; Chough and Sohn, 1990; Dellino and La Volpe, 2000; Dellino et al., 2001; Dellino et al., 2004). As a consequence, hydromagmatic deposits show remarkable variability in grain-size from layer-to-layer and within layers.

* Corresponding author.
E-mail address: Vittorio.VZ.Zanon@azores.gov.pt (V. Zanon).

0377-0273/$ – see front matter © 2008 Elsevier B.V. All rights reserved.
doi:10.1016/j.jvolgeores.2008.09.018

Tuff cones rank among the most common volcanic landforms in the world (Cas and Wright, 1987; Vespermann and Schmincke, 2000; Schmincke, 2004). They are generated during single-stage eruptions, marked by variable degrees of interaction between surface water and ascending magma. Their morphology depends on the variation in the parameters that control the extent of this interaction (e.g. magma supply rate, vent radius, degassing rate, magma chemistry and amount of participating water).

During hydromagmatic eruptions, freshly deposited ash layers are usually rapidly eroded by wave action (e.g. Castro Bank, Azores, 1720 - Machado and Lemos, 1998; Sabrina Island, Azores, 1811 - Chaves, 1915; Ferdinandea/Graham Island, Sicily, 1831 - Washington, 1909; Myōjin-Shō, Japan, 1952–53 - Fiske et al., 1998; Metis Shoal, Tonga, 1995 - Taylor and Ewart, 1997; Home Reef, Tonga, 2006 - Vaughan et al., 2007). A rapid erosion process however, offers the advantage of making large portions of the innermost sectors of these structures accessible to study in order to understand their syn-eruptive depositional processes and the complex contemporaneous and post-eruptive destructive dynamics (Cole et al., 2001; Sohn and Park, 2005; Németh and Cronin, 2007).

The tuff cone of São Roque, in São Miguel Island (Azores) was studied in detail, both at macro- and meso- scales in order to better understand the generation of a volcanic cone and its subsequent destruction.

2. Geological setting

The Azores Archipelago consists of nine volcanic islands that formed in the period from Miocene/Oligocene to Holocene (Johnson et al., 1998; Cannat et al., 1999), above the Azores oceanic plateau in the North Atlantic Ocean. Three major structures define the tectonics of the eastern Azores plateau: the Mid-Atlantic Ridge (MAR) to the west; the East Azores Fracture Zone (EAFZ) to the south, a westward extension of the transcurrent/transpressive Gloria Fault; and the dextral transtensional Terceira Rift (TR) in the northern part of the platform (Machado, 1959; Searle, 1980; Jiménez-Munt et al., 2001) (Fig. 1). The latter is considered to be an ultra-slow spreading rift with an extension rate of 2–4 mm/year (Madeira and Ribeiro, 1990; Gente et al., 2003; Vogt and Jung, 2004).

São Miguel Island, on the eastern side of Terceira Rift, has three caldera lake-dominated volcanoes intersected by fissure systems (or "Waist Zones" - e.g. Booth et al., 1978), characterized by the presence of numerous monogenic basaltic scoria- and tuff- cones as well as tuff rings, along the coasts of the island (Fig. 1).

São Roque tuff cone is located on the southern coast of São Miguel, <1 km west of Ponta Delgada, the islands main town. It is partially embedded within lava flows and is related to the fissure volcanism of "Região dos Picos".

The stratigraphy of Região dos Picos Waist Zone consists of two units identified on the basis of their relative position in respect to the *Fogo-A* member (e.g. Walker and Croasdale, 1971; Booth et al., 1978), erupted from Água de Pau volcano about 4700 years ago (Snyder et al., 2007): *Ponta Delgada* unit that includes all the basaltic lavas and pyroclastic rocks produced before *Fogo-A*, and *Pinhal da Paz* whose formation is more recent than *Fogo-A* and includes basaltic members produced in the last 4700 years, mainly along the central ridge (Ferreira, 2000) (Fig. 2).

The stratigraphy around São Roque tuff cone shows that the lava fountain fallouts of Pico das Faias (to the west), Pico das Canas and associated lavas to the east, as well as the southernmost lava on the shoreline, and São Roque tuff cone itself are older than *Fogo-A* (Ponta Delgada Unit), whereas the other lava flows that cover this area are younger and belong to the *Pinhal da Paz* unit (Fig. 2).

3. Methodology

A preliminary field study was carried out to understand field relationships among the different volcanic structures present in an area of about 9 km^2 surrounding São Roque tuff cone. Relative ages were determined on the basis of the stratigraphic history of the studied area, using the *Fogo-A* deposit as a stratigraphic marker.

Detailed field studies were then carried out on the outcrops of the tuff cone and on the surrounding lava platform, including lithofacies analysis, sampling, determination of bed attitudes, and characterization of fractures (down to about ~2.5 mm wide). An exhaustive analysis of the study area was also performed by aerial photo interpretation.

Field observations were located using a portable GPS receiver with an average precision of ±5.6 m and 1:10.000 scale aerial photos. Geographical data was handled using a 1:25.000 scale topographic map and corrected on high-resolution geo-referenced orthophotomaps.

Studies of the petrographic characteristics of representative hydromagmatic samples were accomplished by binocular microscope analysis.

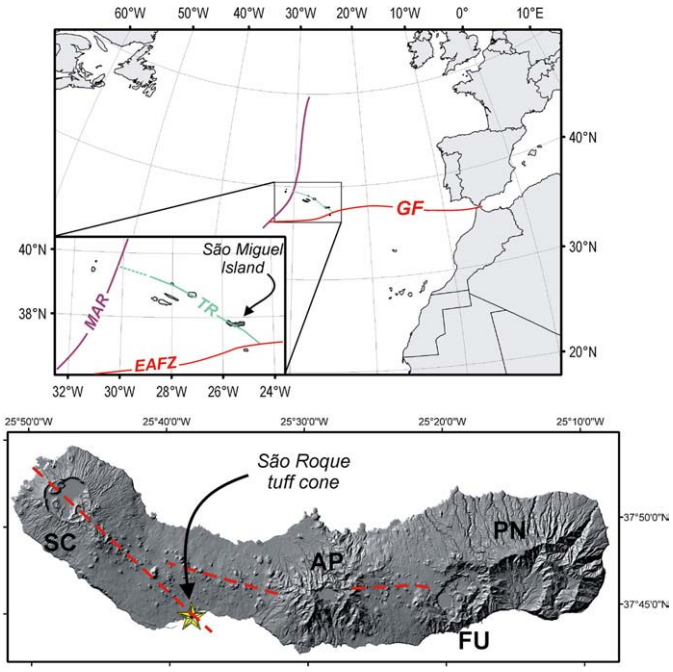

Fig. 1. Map of the Azores archipelago. The uppermost map shows the position of São Miguel Island and its main tectonic features, according to Searle (1980) and Vogt and Jung (2004). The acronyms: MAR stands for Mid-Atlantic Ridge, TR for Terceira Rift, EAFZ for East Azores Fracture Zone, GF for Gloria Fault. The location of São Roque tuff cone is indicated by a star in the digital elevation model of São Miguel Island. Four main volcanic complexes, some of which have caldera lakes, are indicated by acronyms (SC — Sete Citades, AP — Água de Pau, FU — Furnas, PN — Povoação-Nordeste). Dashed lines indicate the areas of structural weakness, characterised by the presence of numerous basaltic monogenic cones.

4. Tuff cone morphology

The tuff outcrop of São Roque has a crescent shape in plan view, opening towards the northeast. It covers an area of about 11,000 m^2 and consists of two main eroded bodies and numerous small islets (each measuring a few square meters), which barely emerge above sea level (Fig. 2a). The eastern and southern sectors of the cone were extensively eroded and no longer crop out.

The largest outcrop (ca 5300 m^2; maximum height 27 m a.s.l.) is located near the village of São Roque and forms a prominent, SW-oriented, morphological structure extending along the coastline. Its depositional units show quaquaversal bedding dips that progressively rotates from SW towards NE, from N35°E to N75°E, with a maximum dip angle of 40° on the inner slopes of the cone. While the outer slopes are smooth, the inner slopes are rough due to numerous fractures and vertical incisions that extend for several meters into the sea. Some small collapse scars and overturned beds are visible here. The south-western edge of this outcrop ends abruptly, exposing a depositional sequence for several meters (Fig. 2b).

The other major rocky body (ca 4900 m^2; maximum height 32 m a.s.l.) is a N–S elongated island that is separated from the lava platform that surrounds the tuff by a 7 m-wide shallow-water channel. The bottom of this channel consists of in-situ pyroclastic rocks, covered by loose blocks of tuff that fell from the above-standing cone, and by meter-sized lava blocks that are part of the adjacent lava platform. In comparison with the former body, this one shows uneven outer slopes that dip westward by 24°–35°, whereas its inner slopes form a vertical cliff. Inward-dipping beds are found (Fig. 2c) only on the southernmost edge of the outcrop.

Between these two main outcrops there are numerous islets arranged along a curved line that emerge for about 50–100 cm above sea level. The side of the islets exposed to the open sea (i.e. towards the east), is truncated, whereas the opposite side gently dips outwards (Fig. 2c).

The present curved rim of the São Roque islets are interpreted as the remnants of the original crater, as indicated by the opposite dipping of layers on the outer and inner slopes.

There are no detailed bathymetric maps of the area; however, divers report that the sea floor around the tuff cone deepens rapidly eastwards, at least to a depth of 8–12 m (i.e. the average depth reached by divers) and it is covered by sand.

5. Facies analysis and interpretation

The São Roque tuff cone consists of a succession of pale-brown to yellow, and occasionally grey, palagonitized and indurated pyroclastic layers comprised of varying proportions of basaltic lapilli and ash. Secondary minerals (i.e. zeolites, calcite and gypsum) are commonly present, and are responsible for the whitish colour of some parts of the tuff cone.

Despite the inaccessibility of the exposures the uppermost deposits could be reached and studied in two adjacent sections (*SR1* and *SR2*; Fig. 3), located on the southern (inner) slope of the northernmost ridge of the cone (Fig. 2a). Section *SR1* is located on the rim of the cone where bed attitude changes its dipping from inwards to outwards in respect to the center of the crater. As a result, the beds that form this section are almost horizontal. Section *SR2*, which is a 2.30-m-high vertical scar, is located on the inner slope of the cone, about 2 m distant from *SR1*. In this section beds normally dip south-eastwards by 23°. In the lower part of the section, beneath an erosion surface, beds show a different attitude.

The deposits of these sections where subdivided into seven lithofacies, as shown in Fig. 3, whose description has been adapted from the nomenclature schemes proposed by Branney and Kokelaar (2002) and Solgevik et al. (2007).

5.1. Lithofacies 1 — lapilli-bearing tuff beds

This is the most abundant lithofacies in the two sections studied. It consists of a succession of yellow lapilli-bearing, coarse ash beds of variable thickness and grain size (Fig. 4a). These beds are laterally continuous, and thin over steeper slopes. Individual beds are commonly reverse graded and are delimited by erosion surfaces and diffuse layering of coarse grains. Juvenile lapilli (∅=2.0–3.5 cm) are rounded, dense, non-vesicular and form discrete, continuous layers within the beds, or 3-to-5-cm-thick lenses, which are either massive- or reverse- graded. Angular lava lithics and irregularly shaped vesicular juvenile clasts (volcanic bombs) are also found.

Bomb sags 4 to 6 cm deep are numerous, whereas in the ash layers on the inner slopes of the cone there are several large bomb sags (∅=30–35 max cm) that still contain dense bombs. Many large cow pat bombs (∅=15-35 cm) are found plastered on the inner slopes. In some places this lithofacies grades into lithofacies 2.

5.1.1. Interpretation

Similar lithofacies were described by other authors (e.g. Wohletz and Sheridan, 1979; Fisher and Schmincke, 1984; Wilson and Hildreth, 1998; Valentine and Fisher, 2000; Cole et al., 2001; Solgevik et al., 2007) who interpreted them as fallout deposits, pyroclastic surge or co-surge fallout deposits. However, as regards São Roque tuff cone, the following explanations are proposed: (1) contemporaneous deposition of ash beds by pyroclastic surges (proximal facies) during continuous ash and ballistic fallout, concurrent with grain-flow processes, as suggested by common inverse grading and lateral pinching out of some lapilli layers (Sohn and Chough, 1993) and; (2) oscillations between magmatic and hydromagmatic fragmentation. This assumption is supported by the hybrid character of the thin pinch-and-swell lenses within the laterally continuous layers and also by the coexistence of fine hydromagmatic ash, cow pat bombs and vesicular lapilli. Evidence of contemporaneous hydromagmatic and magmatic fragmentation were also reported for hydromagmatic eruptions, such as Surtsey (Iceland, 1963–67) and Capelinhos (Azores, 1957–58), which show that surge and fall depositions were contemporaneous in the emergent stage of many tuff cones (Machado et al., 1962; Thorarinsson et al., 1964; Moore et al., 1966; Moore, 1967; Thorarinsson, 1967; Camus et al., 1981; Fisher et al., 1997; Cole et al., 2001; Schmincke, 2004).

5.2. Lithofacies 2 — stratified lapilli

This lithofacies is moderately common in the stratigraphy of São Roque tuff cone. It shows two different kinds of beds: (1) continuous and planar clast-supported beds, commonly poorly sorted and seldom formed by grey-coloured agglutinated fragments (Fig. 4b). This former feature is rare and predominantly vesicular and glassy class (∅=2.5–3.5 cm) are stuck together by plastering. The thickness of the beds is typically less than 5 cm; (2) Stratified or massive lapilli layers alternating with a few thin ash layers. They mantle the pre-existing surface with 15 to −20-cm-thick deposits and commonly grade into ash-supported lapilli layers. The boundary between these lapilli layers and the underneath ash layers is frequently an erosion surface. Lapilli layers are constituted by unwelded juvenile clasts commonly sub-round (∅=1.2–3.0 cm) angular lithic lava clasts (∅=1.2–2.5 cm), and loose crystals of olivine and pyroxene. Vesicular cow pat bombs (∅=4–6 cm) and dense lava lithics of equivalent size are widespread on the surface of these layers. A single 35-cm long fractured dense bomb was found near the base of the sequence.

5.2.1. Interpretation

Vesicular lapilli beds are interpreted as very proximal fallout deposits produced by continuous Strombolian explosions. The faint erosion surfaces at the base of the layers are probably due to highly diluted surges, caused by the air waves produced by the expansion of gases during blasting (Zanon et al., in press). This lithofacies was produced when sea water had no access to the disrupting magma and the eruption was driven by magmatic fragmentation.

5.3. Lithofacies 3 — diffuse-stratified tuff

This lithofacies is found as a 35-cm- thick, complex depositional sequence near the base of *SR1*, whereas in the upper part of *SR2* it is present as two distinct beds, with a total thickness of about 50 cm. It is characterized by planar bedding with alternating continuous and discontinuous diffuse stratification. It is made up mainly of palagonitized ash (Fig 4c) and clasts arranged in discontinuous trains or lenses or, seldomly, dispersed within the matrix. Trains are commonly less than 0.8 cm thick and only a few cm long. Clasts have various dimensions and are composed of vesicular lapilli, fragmented bombs, angular lava lithics, fragments of pre-existing tuff, crystals and oxidized clasts. On steep slopes, this lithofacies shows thinning and its matrix forms thin planar laminae and lapilli-bearing lenses.

5.3.1. Interpretation

These tuff beds are typically interpreted as facies of intermediate-to-proximal deposits from pyroclastic surges (e.g. Wohletz and

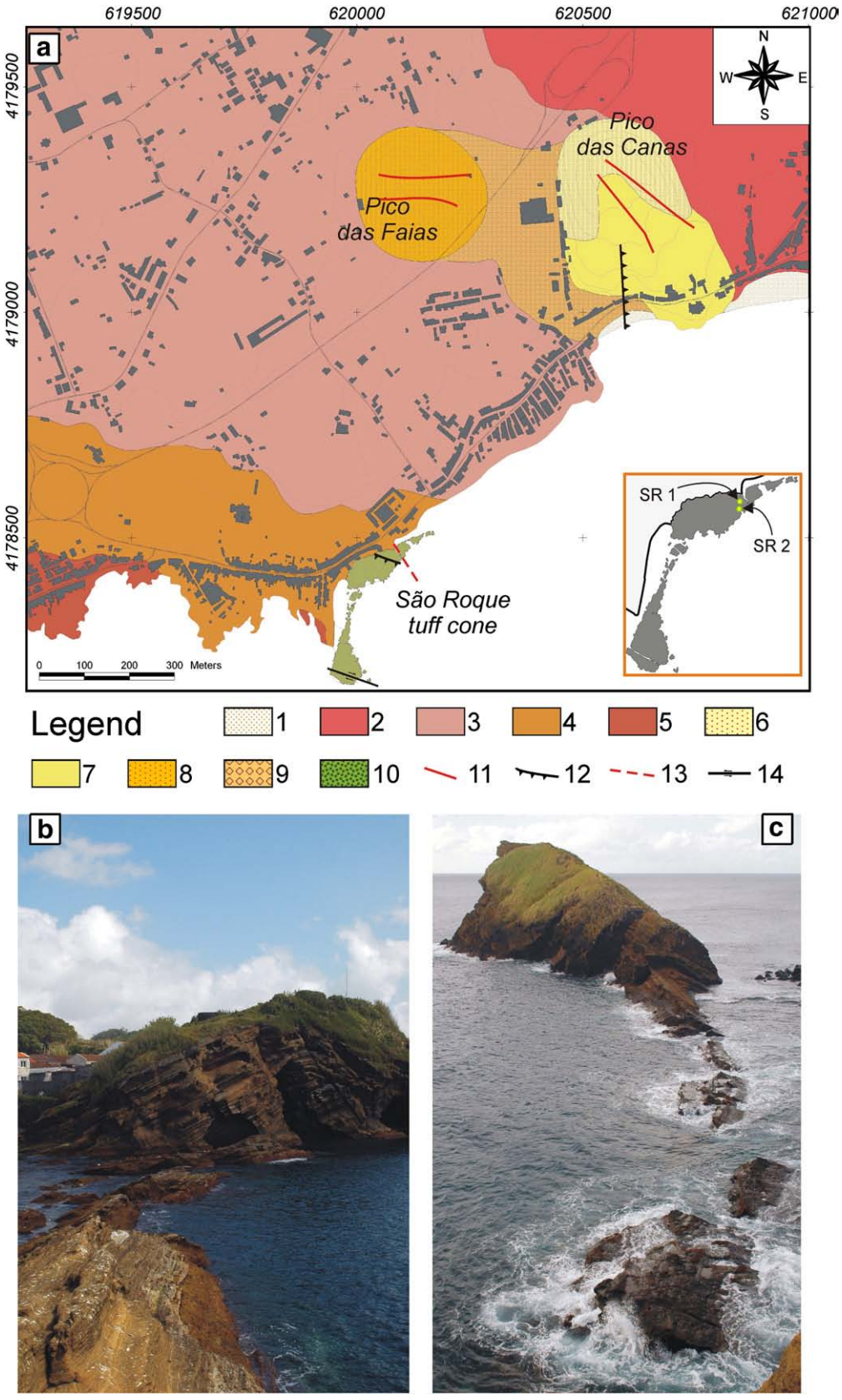

Fig. 2. (a) Simplified geological map of the area around São Roque tuff cone. The legend reports: [1] recent beach sand; [2] undated recent basaltic lava flow. Deposits aged between 2470 and 4700 years BP are: [3] basaltic lava flow and [4] upper basaltic lava platform. Deposits older than 4700 years BP are represented by: [5] lower basaltic lava platform; [6] scoriaceous tephra from Pico das Canas and [7] related lava flow; [8] proximal and [9] distal tephra fallout from Pico das Faias; [10] São Roque tuffs. Tectonic lineaments are: [11] fractures; [12] normal faults; [13] supposed normal faults; [14] transcurrent fault. In the inset it is shown the location of the two stratigraphic logs. (b) View of the northern sector of the cone dissected by N60°E trending fractures. (c) Photograph taken from the top of the northern rocky body, showing the southern outcrops of the tuff cone, consisting of small submerged rocks and islets.

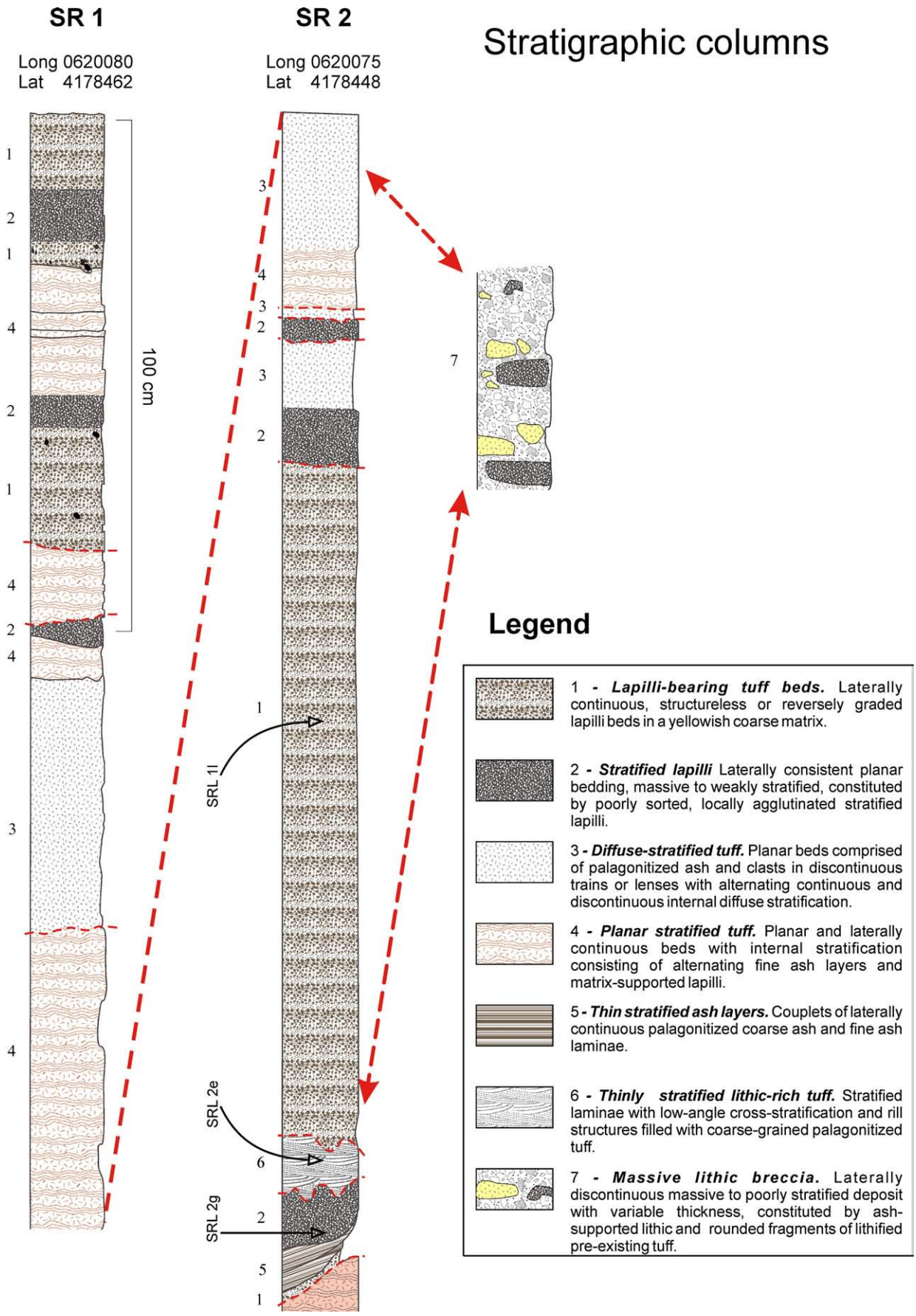

Fig. 3. Schematic stratigraphic columns showing the distribution of seven lithofacies. Thin dashed lines indicate erosion surfaces. The collection location of the three representative specimens shown in Fig. 8 is also indicated. At the distance of about 8 m eastwards, the *SR2* sequence is laterally substituted by lithofacies 7. Coordinates are in UTM zone 26S.

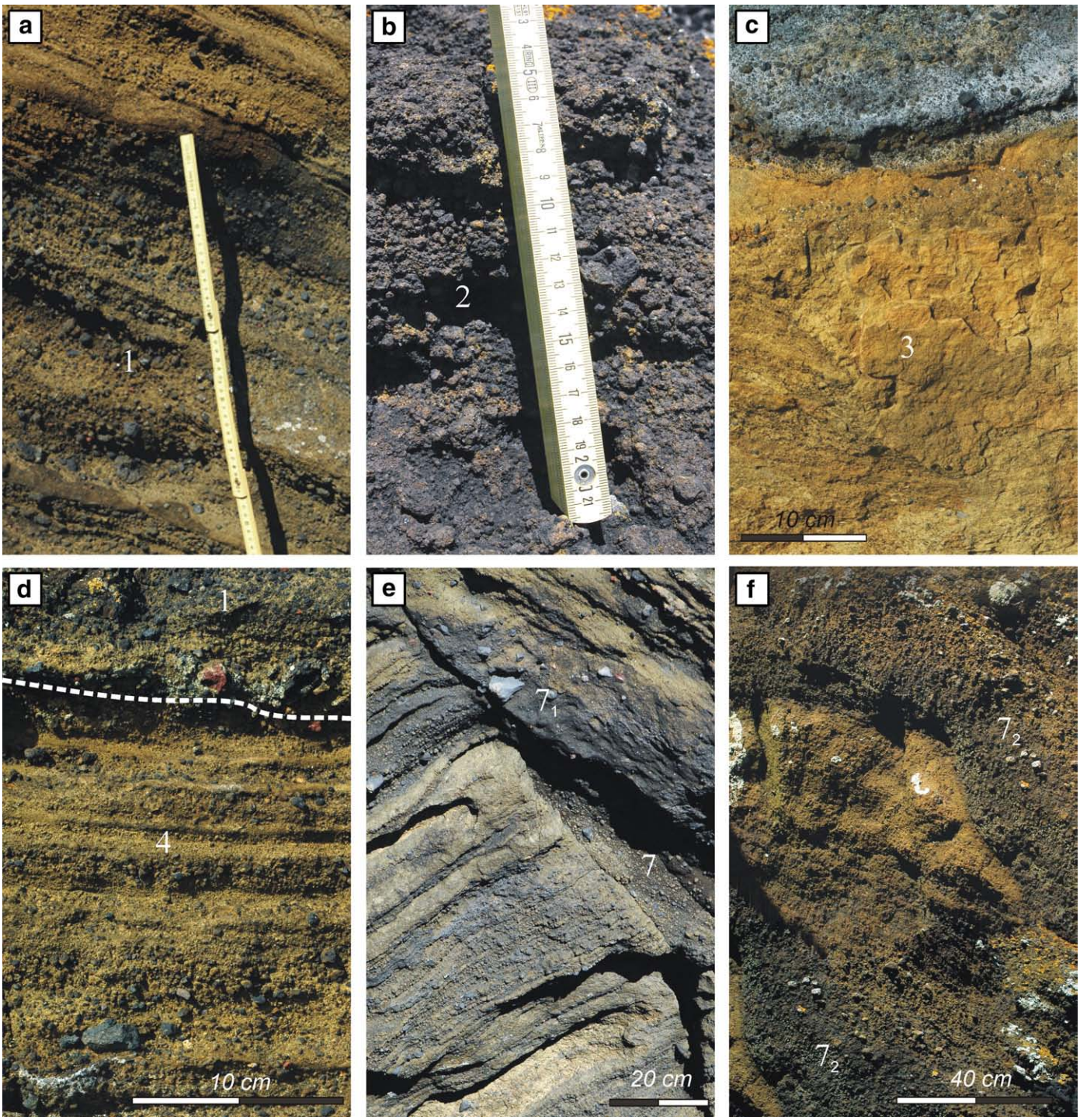

Fig. 4. Characteristics of pyroclastic deposits in the São Roque tuff cone. (a) Most of the outcrops are represented by lithofacies 1, which is made up of a succession of lapilli-bearing tuff beds that have a mixed hydromagmatic surge and fall origin. (b) Stratified lapilli fallout and agglutinated scoria constitute lithofacies 2, which is present as numerous interbedded layers of varying thickness, sometimes grading into lithofacies 1. (c) Diffuse-stratified tuff of lithofacies 3, containing trains of lithics and/or non-vesicular lapilli, representative of proximal pyroclastic surge deposits. (d) Lithofacies 4 is composed of an alternation of stratified clast-supported layers and laminated ash layers, interpreted as a medial-to-distal deposit produced by hydromagmatic surges and contemporaneous fallout. (e) Lithofacies 7_1 is the massive-to-poorly stratified muddy unit related to syn-eruptive intra-crater landslides. It lies unconformably on a erosive surface of the pre-existing flank slopes or on hybrid lithofacies 7. (f) Lithofacies 7_2 is a clast-rich matrix-supported unit containing common intraformational tuff clasts of different types. Evidences of flowage are widespread all over the outcrops and erosion of the embedded fragments is common.

Sheridan, 1979; Fisher and Schmincke, 1984; Cas and Wright, 1987; Carey, 1991; Branney and Kokelaar, 2002). Grain-size variations, the presence of discontinuous layers and lenses and thinning are considered to be clear signs of changes in depositional conditions (e.g. high shear stress, velocity, flow steadiness and particle concentration) which, in turn, suggest the existence of turbulent conditions during the emplacement of these diluted pyroclastic density currents (Sigurdsson and Fisher, 1987; Cole and Scarpati, 1993). The presence of palagonitized basaltic ash confirms the hydromagmatic character of this lithofacies (e.g. Bonatti, 1965).

5.4. Lithofacies 4 — planar stratified tuff

This lithofacies is somewhat similar to lithofacies 1 and is composed of planar and laterally continuous beds with internal stratification that consists of alternating fine ash layers and matrix-supported lapilli layers 3 to 7 cm thick (Fig. 4d). Lapilli layers are commonly stratified and show both normal and reverse grading, although in some places they are just single trails of poorly sorted clasts. Finer clasts (∅=1.5–2.5 cm) are commonly angular and non-vesicular and consist mainly of lava lithics and, secondarily, of dense juvenile lapilli. Coarser clasts (∅=4.0–6.5 cm) comprise lava lithics and poorly-vesicular juvenile bombs, but some small oxidized scoria and fragments of exotic tuff are also present. The matrix is made up of palagonite with fragments of olivine, clinopyroxene and plagioclase settled along the c-axis and by scattered weathered vesicular lapilli (∅<0.5 cm). Ash layers are 1– 3– cm thick and are laterally continuous. Small folds frequently occur probably due to the plastic deformation of ash during consolidation, and it is possible to find also some small (3–5 cm-deep) fill-in structures composed of fine-to-coarse ash. Planar lamination is sometimes visible in the less palagonitized layers; otherwise the matrix looks generally massive. Commonly the contact between layers is sharp and non-erosive, although there are also gradational and diffuse boundaries.

5.4.1. Interpretation

On other volcanoes similar deposits were interpreted as fallout deposits or as pyroclastic surge and co-surge fallout deposits, due to the contemporaneous presence of characteristics normally pertaining to both fallout and surge deposits (e.g. Wohletz and Sheridan, 1979; Fisher and Schmincke, 1984; Cole et al., 2001; Dellino et al., 2004).

It is difficult to discriminate between the two depositional mechanisms, especially in the absence of a large number of outcrops. Nevertheless, a single couplet constituted by both coarse and fine-grained layers is interpreted as deposited from a single surge (Sohn and Chough, 1989; Dellino et al., 2004) and This lithofacies is interpreted as inferred to be a medial-to-distal deposit from hydromagmatic surges and concurrent simultaneous fallouts.

5.5. Lithofacies 5 — thin stratified ash layers

This lithofacies is the least abundant in the studied sections. It consists of laterally continuous, thin grey-to-yellowish ash layers. It comprises couplets of coarse ash and, less palagonitized, fine ash laminae. The thickness of both coarse and fine ash laminae ranges widely from 0.4 to 1 cm. Contacts between the coarse and fine ash layers are either sharp or gradational.

This lithofacies is formed by two different depositional beds, resembling a half-lens, and with a total maximum thickness of 25 cm. They are found at the base of *SR2*, are not separated by any erosive surface. Their bedding is different from the layers above and below.

5.5.1. Interpretation

These stratified planar ash layers are typical of distal pyroclastic surge deposit of hydromagmatic eruptions in tuff cones and tuff rings (Cas and Wright 1987). We suggest that syn-eruptive sliding and tilting of portions of the inner slope of the cone might be involved in the present bedding, different from the layers above and below.

5.6. Lithofacies 6 — thinly stratified lithic-rich tuff

This lithofacies is rare in the two studied sections and consists of numerous grey coloured planar laminae with low-angle cross-stratification and rill structures (U-shaped channels) filled with coarse-grained tuff. There are no vesicular lapilli but small angular lava lithic clasts (∅<0.8 cm) and crystal fragments (∅<0.4 cm) are present, dispersed within a partially palagonitized ashy matrix. The thickness of each lamina ranges from 1 cm to a few mm, totaling about 25 cm. The boundaries of this lithofacies are characterized by erosion surfaces.

5.6.1. Interpretation

Low-angle cross-stratification is a typical feature of deposits formed by turbulent pyroclastic density currents with a low particle concentration (Fisher and Waters, 1970; Sohn and Chough, 1989; Sohn and Chough, 1992) found in tuff cones/rings, not too far from the source (Chough and Sohn, 1990; Sohn, 1996; Sohn and Park, 2005). This lithofacies is interpreted as being constituted of proximal-to-medial deposits from pyroclastic surges.

5.7. Lithofacies 7 — massive lithic breccia

This lithofacies is laterally discontinuous and is only present in the inner part of the crater, where it forms a steep slope dipping inwards, lying unconformable over eroded beds dipping outwards. In some places, it shows plastic deformation where it covers the irregularities of the underlying layers. Contact with the other lithofacies always occurs through an erosive surface. Lithofacies 7 is constituted of variable amounts of lithics contained in an ash matrix. It is massive–to-poorly stratified, shows variable thickness and contains rounded fragments of older tuff. Two units, separated by an erosion surface, were recognized on the basis of their matrix/coarse -clast ratio. Unit 7_1 appears as a massive-to-poorly stratified, grey, muddy ash, with smooth irregular surfaces showing clear evidence of plastic deformation. It contains sparse angular lava lithics of different size (∅>9.5 cm) without tractive structures (Fig. 4e). Close to the base, clasts of smaller size show a poorly developed imbrication.

Unit 7_2 is a clast-rich, matrix-supported, moderately-sorted deposit lying below unit 7_1. It is massive-to-poorly cross-stratified and individual beds show internal normal grading. Clasts are brown to grey-coloured, lithologically heterogeneous (vesicular juvenile lapilli and lava lithics) and range from angular to sub-rounded, normally with a reduced grain size (∅<3 cm). It shows variable thickness and is sometimes present as large lenses which plastically embed large fragments of tuff (up to 120 cm in length) from other lithofacies. The embedded tuff is eroded all around its boundaries, showing curved and smooth surfaces (Fig. 4f).

5.7.1. Interpretation

Both these units are interpreted as deposits from syn-eruptive collapses forming debris flows or slumps generated by the remobilization of wet tephra (e.g. Sohn and Chough, 1992; Cole et al., 2001; Sohn and Park, 2005; Zanon, 2005; Németh and Cronin, 2007). They can easily erode and carry large tuff boulders.

The difference between the two units is mainly due to different transport conditions. Grain-size, structure and texture suggest depositional conditions typical of a hyper concentrated flow for the lower (7_2) unit and of a debris flow for the upper unit (7_1).

6. Location of source vents

The attitude of beds definitely indicates the source of explosions. In the absence of a pre-existing morphological relief, no predominant wind conditions and a small localized vent, all deposited strata have the same radial dip direction (either inwards or outwards), whereas the presence of pre-existing morphological structures may well have influenced flow direction of pyroclastic density currents, considerably changing bed attitude.

As regards São Roque tuff cone, bed attitude changes both along the crater rim and vertically, across some stratigraphic sections, and at least one major unconformity surface exists at the base of the *SR2* section, clearly indicating that the source location progressively shifted. Bed attitude on the island, measured from the south to the

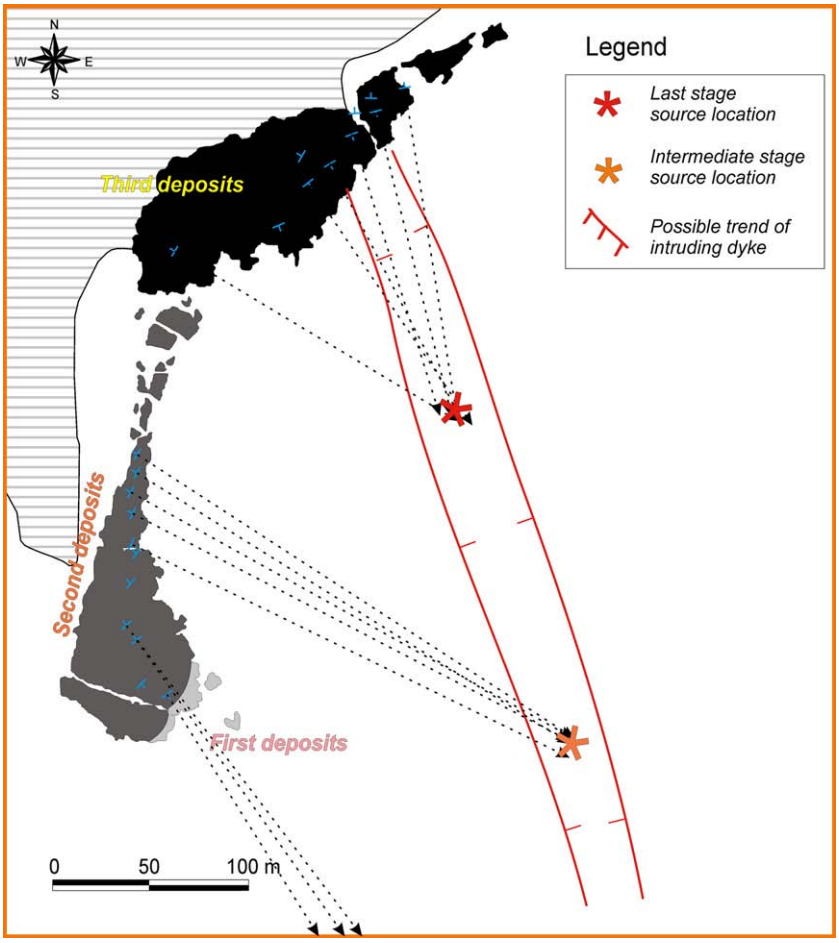

Fig. 5. Inferred position of the intruding dyke, obtained from the projection of the attitude of selected beds measured in various locations. Stars show the probable vent source obtained from the intersection of the majority of the projections of bed attitude. The different grey colours indicate the deposits with different beddings that are probably related to the various phases of the eruption.

north, almost following the same stratigraphic level, reveals a progressive eastward rotation. On the basis of these considerations, a possible vent source was located at about 230–240 m SE of the group of islets (Fig. 5).

On the main outcrop bed attitude was measured on the deposits from the last stage of the eruption, corresponding to the sequence which lies unconformably over the inner slopes of the tuff cone, and revealed that another source vent was possibly located at about 120 m SE of the outcrop.

Evidence suggests that during the course of the eruption São Roque had several sources aligned along a NNW–SSE trending fissure (Fig. 5), and the stratigraphic position of the layers is consistent with a migration of the vents from SSE to NNW. This is in agreement with the regional fracture pattern of the Waist Zone in this area, as reported by Ferreira (2000) and also evidenced by some morphological features of the surrounding cinder cones (Corazzato and Tibaldi, 2006).

7. Fractures and faults

São Roque tuff cone outcrops are crossed by numerous fractures and faults responsible for the dissection of the cone and the formation of numerous abrupt truncations with the consequent exposure of the innermost part of the cone. They consist of single cracks, which appear to be arranged along a definite direction at a macro scale, whereas they normally follow a zigzag pattern around grains at a meso scale. Many of them are 0.5–1 cm wide and are filled with fine debris of uncertain origin, while others are quite fresh and empty, which probably suggests a recent movement. On the basis of the strike and dip variations, it is possible to recognize various types of faults/fractures all along the outcrops (Fig. 6a).

7.1. Radially-arranged fractures

These are the most common fractures. They are long enough to cross the cone all through its horizontal extension and deep enough to allow sea water to flow into them. Most of them show only one vertical component with a minor displacement (generally within 4 cm) and are present on the two main outcrops. Other radial fractures reveal only horizontal movements, with major displacements (up to 1.8 m) or show a transtensional component with minor vertical displacement. They generated numerous islets which show lateral displacement. These fractures are aligned radially from N15°W in the northern outcrop to N80°W in the southern outcrop and are prominent in the vertical exposure of the southern cliff of the major rock body (Fig. 7a). In rare cases a conjugate joint system developed major vertical collapses and rock falls, but the length of these fractures is limited. Many radial fractures, with a vertical dip and a limited displacement are also present on the exposed wall of the lava flow platform, showing the same trend observed in the tuff nearby.

7.2. Tangentially-arranged fractures

This type of fractures is less common and is usually associated with small collapses. These fractures are represented in the rose diagram of Fig. 6a. Their directions range from N50°W to N60°E, and they show a limited development (only in rare cases their length exceeds 15 m).

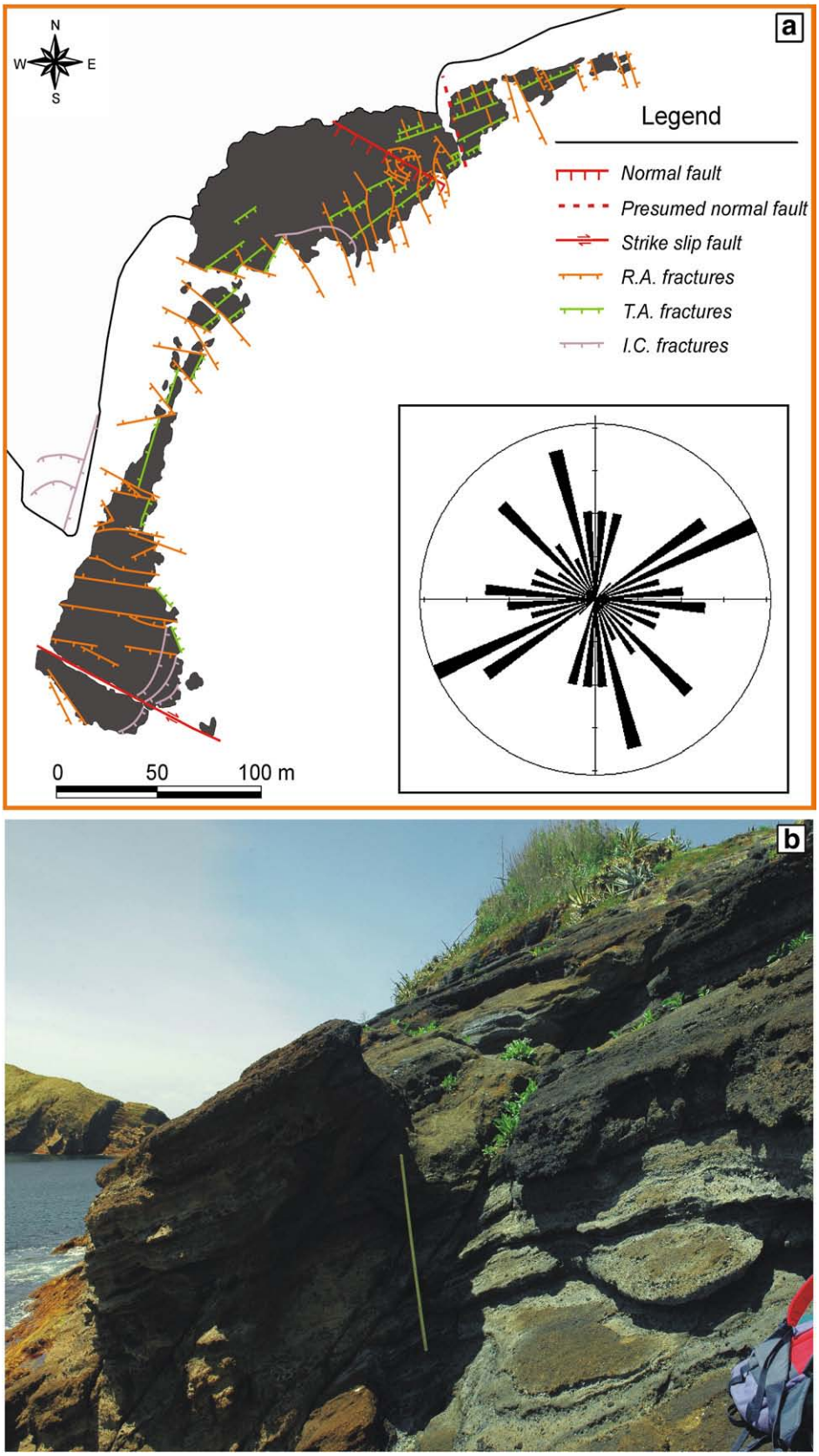

Fig. 6. Structural framework of the tuff cone evidenced by faults and fractures (6a). R.A. fractures, T.A. fractures and I.C. fractures stand for radially-arranged fractures, tangentially-arranged fractures and incipient collapse fractures, respectively. The dilatational fractures could not be mapped because of their reduced size and their local distribution. The rose diagram shows the orientation of the fractures. The gap zone in the rose diagram between N20°E and N50°E is an artefact due to the lack of data from the eastern and southern portions of the cone. Tectonic activity started after the end of magmatism and developed along NW–SE, NNW–SSE and WNW–ESE trending directions (6b) dissecting the cone and contributing to present-day morphology.

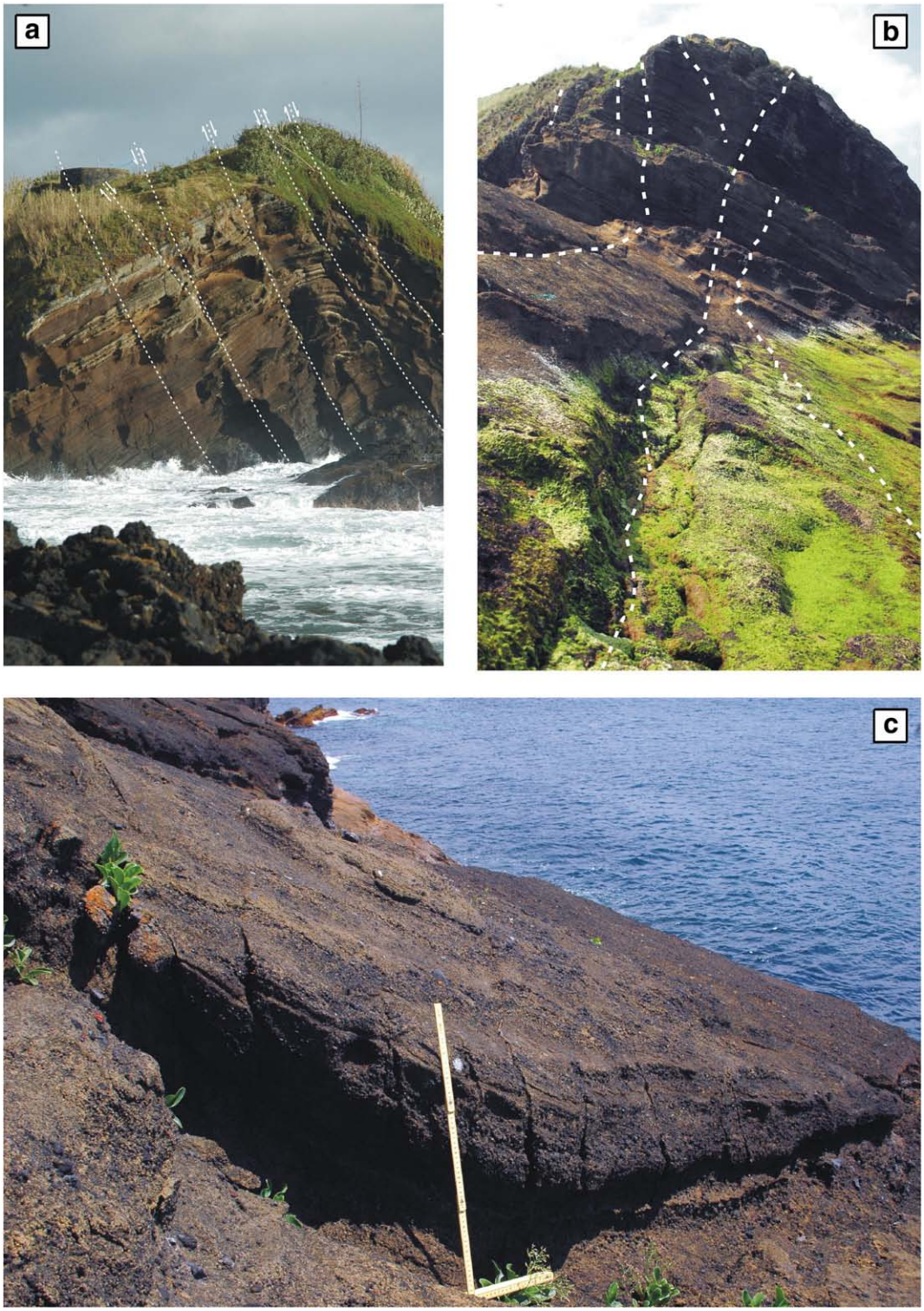

Fig. 7. Different types of fractures on the cone. N60°E trending fractures dipping towards SE with a reduced displacement (<4 cm on average) are the most common fractures on the cone and are associated with basement failure and flank collapses. The picture in Fig. 7a shows the southern cliff of the main rocky body, seen from the main island. Other radial fractures showing a transcurrent movement are instead responsible for major displacements. Tangential fractures (7b) are less common are usually associated with small adjustments in the tuff bodies in response to flank failures. Dilatational fractures are well localised and shallow and are caused by the diagonal cracking of a lapilli-bearing deposit in response to the plastic deformation of the underlying layer along a steep slope (7c). This type of fracture is present in a bed located in the central sector of the main rocky body, lying on inward-dipping slopes.

Usually these fractures exhibit only a vertical component with a reduced displacement (<15 cm) (Fig. 7b) and are located both on the inward- and outward-dipping flanks of the cone with an opposite attitude. Others are located close to the rim of the cone, following its curved shape and forming a sort of *en enchelon* structure. They truncate all sides of the islets.

7.3. Incipient-collapse fractures

These fractures are up to 2–3 m long curvilinear cracks, about 0.5–1 cm wide. They are present only on the southern tip of the main island, on the surface of protruding pyroclastic sequences which lie on steep slopes, cut by vertical tangentially-arranged fractures. They

delimit the scar left by landslides (small sector collapses) or areas prone to collapse.

7.4. Dilatational fractures

These form a set of parallel and locally developed fractures that are too small to be represented on the rose diagram. They appear only in a small section of some lapilli-bearing pyroclastic beds (lithofacies 1) and are orthogonal to the maximum dip of the beds (Fig. 7c). They measure 10 to 100 cm and show a vertical displacement of <3 cm with a transtensional, or more rarely, a transpressive component. They become progressively wider (up to 1.2 cm) towards the base of the bed. These fractures were seemingly caused by the down-sag deformation of the underlying bed in a semi-plastic fashion (unconsolidated). The overlying unit accommodated the strain in a semi-brittle fashion, and experienced fracturing.

7.5. Faults

One major fault (N60°W strike, dipping 55°S) crosses the main outcrop, with a vertical displacement of ~8 cm (Fig. 6a, b) and is currently contributing to the seaward sliding of some sectors of the cone. Another fault (N15°W) appear to be concealed in the northern side of the main outcrop. It is most probably subvertical, with an estimated downthrow of 12 cm towards the East. Its fault plane was eroded by the ocean, which caused the enlargement of the fractured area and its erosion, generating a more than 120 cm-large fracture. Finally, a vertical dextral-strike slip fault cuts through the southern tip of the cone, with a displacement of 4 m towards WNW.

These structures were active between the end of the volcanic activity and the emplacement of the lava platform where, indeed, no displacement is visible either in its northern nor in its western sectors.

8. Landslides and instability of deposits

The remnants of the tuff cone show evidence of several phases of reworking and erosion of the deposits: sin-eruptive processes, syn-eruptive to immediate post-depositional processes and post-lithification processes.

Syn-eruptive remobilization is indicated by the presence of hyper concentrated flows and debris flows found on the inner part of the cone, as described in lithofacies 7. These deposits form inward dipping slopes, lying unconformable over eroded beds dipping outwards, and indicate (1) the occurrence of cone destruction/collapse events, as indicated by the eroded layers and (2) the reworking of superficial layers as indicated by the inward sliding of deposits.

Unconformable layers as described in lithofacies 5 may also result from syn-eruptive sliding and tilting of portions of the inner slope of the cone.

Syn-eruptive to immediate post-depositional processes refers to events that cannot be constrained to a syn-eruptive period but developed before the lithification of the deposits. At São Roque these processes corresponds to small-scale slides, originating slumping folds due to the plastic deformation of wet ash, as described in lithofacies 4.

Post-lithification processes include the development of a network of fractures that greatly reduced the resistance of the tuff cone. These weakness planes and the erosion inflicted by the sea waves accelerated the development of a range of debris-falls and block-falls, from small-scale events to large block collapses that produced quite evident collapse scars and greatly contributed to the present complex morphology of the cone.

These erosive processes are still in progress, mainly along incipient-collapse fractures and vertical radially-arranged fractures, as indicated by the blocks and debris deposits found around the cone.

The coastline of São Miguel Island in the proximity of the tuff cone is rectilinear and does not offer protection against the action of the ocean. For this reason, the cone has been exposed to wave erosion since its emergence (>4700 years B.P.), before being partially covered by more recent lava flows coming from the north (post *Fogo-A* eruption, i.e. 4700 years ago). Although lava surrounded the northern and western sides of the cone, wave action was still able to remove it from the tuffaceous slopes and isolate the remnants of the cone. Presently, loose blocks of lava fill the channels and protect what remains of the cone.

9. Palagonitization of deposits

All the rocks of the São Roque tuff cone show a high degree of consolidation due to the extensive palagonitization of sideromelane glass. Even fallout-related deposits are consolidated due to the contemporary deposition of fine hydromagmatic ash and the presence of clots of acicular zeolites filling in lapilli vesicles.

In some samples (Fig. 8a), where the weathering process has not affected the crystal population (Fig. 8b), it is possible to distinguish two types of palagonite, as described by Peacock (1926) and Zhou and Fyfe (1989). Gel palagonite is dark brown, translucent and isotropic; fibrous palagonite is orange or yellow, transparent, birefringent and fibrous and it may also contain spherical protocrystallites (Fig. 8c). The latter, if in great numbers, can form a spongy texture which is characteristic of a mature stage in the alteration process (Thorseth et al., 1991). A temporal relationship links these two types of palagonite: immediately after the emplacement, glass starts to dissolve forming gel palagonite. Gel palagonite is then replaced by fibrous palagonite (Zhou and Fyfe, 1989). This process is coupled with the formation of secondary minerals (mainly zeolites and calcite) and clay (Fig. 8d), which fill the voids, and small fractures inside the palagonitized mass.

10. Basement

The only source of information on the basement of the São Roque cone are accidental blocks ejected during the eruption. Two types of accidental lithic clasts were recognized: lava and consolidated pyroclastic rocks (tuff). These are widespread all over the slopes of the cone, but they are not equally distributed in a vertical stratigraphic section.

In the lowermost section of the stratigraphic sequence, close to sea level, pyroclastic beds are characterized by the diffuse presence of small (<15 cm across) basaltic lava clasts (Fig. 9a). These are angular, non-vesicular, poorly weathered and zeolite-free and contain a large amount of olivine and minor pyroxene (Fig. 9b). They clearly represent samples of a basaltic lava flow from an ancient eruption.

On top of the upper tuff cone sequence, numerous tuff blocks are present in bomb sags (Fig. 9c). They are relatively large (max 55 cm in diameter), rounded and extensively palagonitized and zeolitised. They are also yellowish-to-brown coloured and contain rounded vesicular lapilli, oxidized scoria, large pyroxene and olivine crystals, and various small angular fragments of lava, similar to those found in bombs in the lower parts of the succession (Fig. 9d). These are interpreted as fragments of tuff from older submerged hydromagmatic centres.

11. Discussion

In consideration of the geological features discussed throughout this study, namely stratigraphy, attitudes of the beds, and the constitution and structure of the deposits, São Roque is considered to be a composite tuff cone, despite the reduced dimensions of its outcrops. It has developed a complex morphology due to the action of several syn-eruptive (alternated constructive and destructive phases) and post-eruptive processes.

11.1. Building of the cone

The eruption of São Roque started offshore São Miguel Island and vents migrated from SSE to NNW, along a dyke that progressively

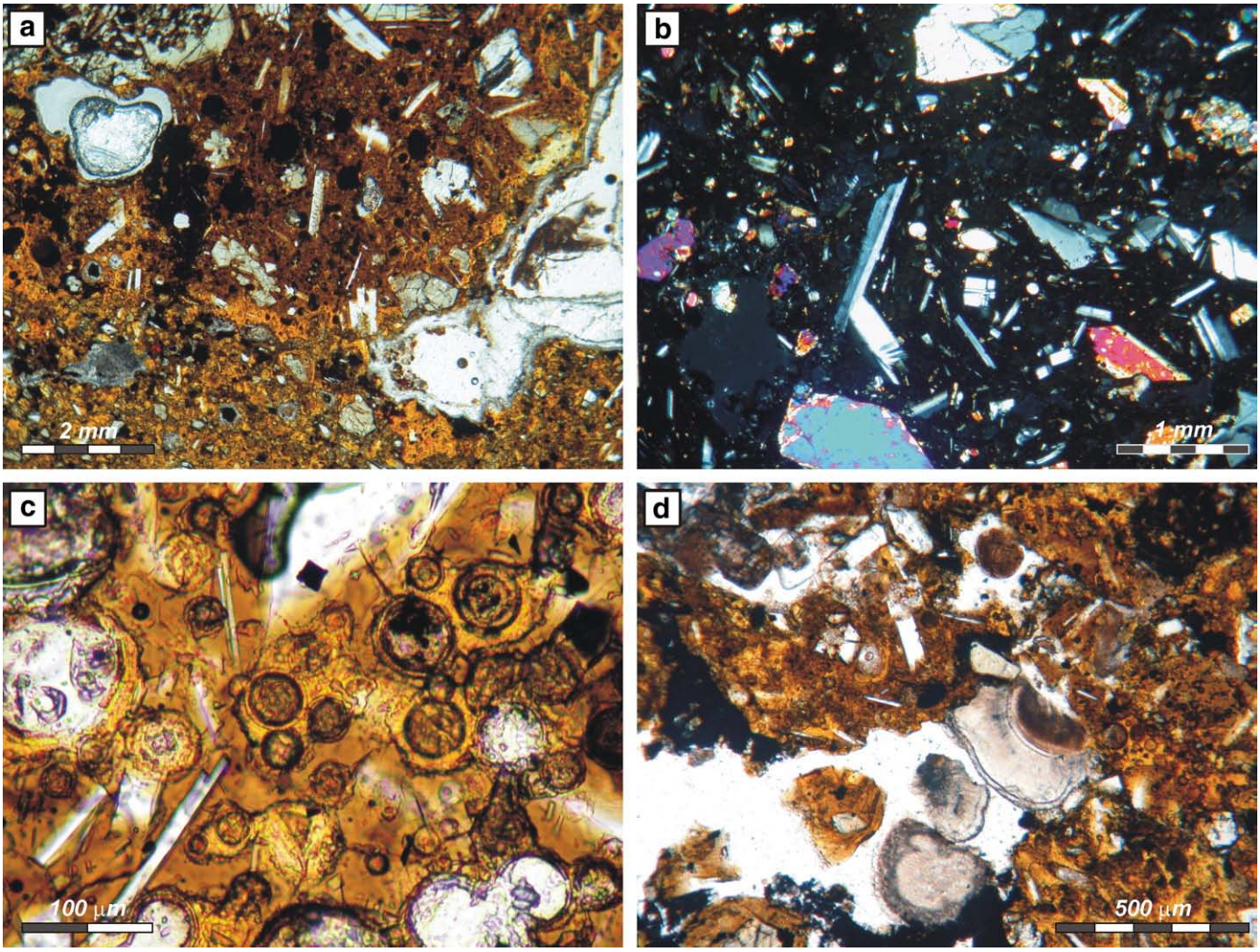

Fig. 8. Petrographic features of selected samples from the two stratigraphic sections. Coexistence of gel and fibrous palagonite within the SRL 1L sample (8a). Un-weathered fragments of clinopyroxene, olivine and plagioclase are also evident, whereas numerous tiny (<0.15 mm) crystals of the same kind are dispersed in the palagonitized glass (8b). This picture, taken under crossed nicols, shows how the texture of these rocks is not due to flowage after emplacement because iso-orientation of tabular minerals (plagioclase) is lacking. Globules are produced during early stages of palagonitization (Thorseth et al., 1991) and their presence in clots or trails is indicative of a late stage process – Sample SRL 2E (8c). Calcite crystals, also of considerable size, are commonly present in all studied samples as globular crystals. They occupy fractures and voids and are sometimes found together with zeolites – Sample SRL 2G (8d).

intruded towards the NNW, as indicated by stratigraphic relations and bed attitude, which allowed descrimination the first deposits on the south-easternmost end of the island from the most recent ones on the main outcrop.

The initial shape of the cone resulted from the accumulation of tephra around the vents caused by explosive hydromagmatism (lithofacies 1, 3, 5, 6), which generated pyroclastic density currents that were seldom followed by purely magmatic explosive activity (lithofacies 2), generating tephra fallout. This alternating deposition of "wet" and "dry" tephra (i.e. hydromagmatic ash layers and clast-supported lapilli layers) occurred for a short time in the history of the cone, and were soon replaced by other phases of "wet" deposition (lithofacies 3, 4).

11.2. Destruction of the cone

Small syn-eruptive intra-crater landslides commonly occur both in scoria and tuff cones and are mainly associated with the natural repose angle of the pyroclasts and the amount of water adhering to the particles or trapped between them. At São Roque, syn-eruptive intra-crater landslides and post-eruptive debris-falls and block-falls contributed to the present morphological structure of São Roque cone. Regarding the extensive destruction observed at São Roque tuff cone, further consideration should be given to the destabilizing effect of the rapid accumulation of tephra over a possibly steep morphological submarine relief (a pre-existing tuff cone). In this case, it is possible that water-saturated sediments formed highly unstable deposits which continuously slumped forming submarine debris-flows or, alternatively, there may have been a post-eruptive lateral spreading of a brittle basement below the tuff cone. However, the orientation and type of fractures and the faults observed in the cone do not match the models suggested by Delcamp et al. (in press) to explain lateral spreading.

11.3. Formation of fractures and faults

Extensional and shear fractures, common in many scoria and tuff cones, develop in response to shallow dyke intrusions and/or magma breakouts (e.g. Gudmundsson et al., 1999; Lanzafame et al., 2003; Engvik et al., 2005; Gudmundsson and Loetveit, 2005). Evidence of the shallow emplacement of an intruding dyke during São Roque eruption is the alignment of vents along the NNW–SSE regional trend. The stress caused by craterization induced incipient fracturing in the lithologies

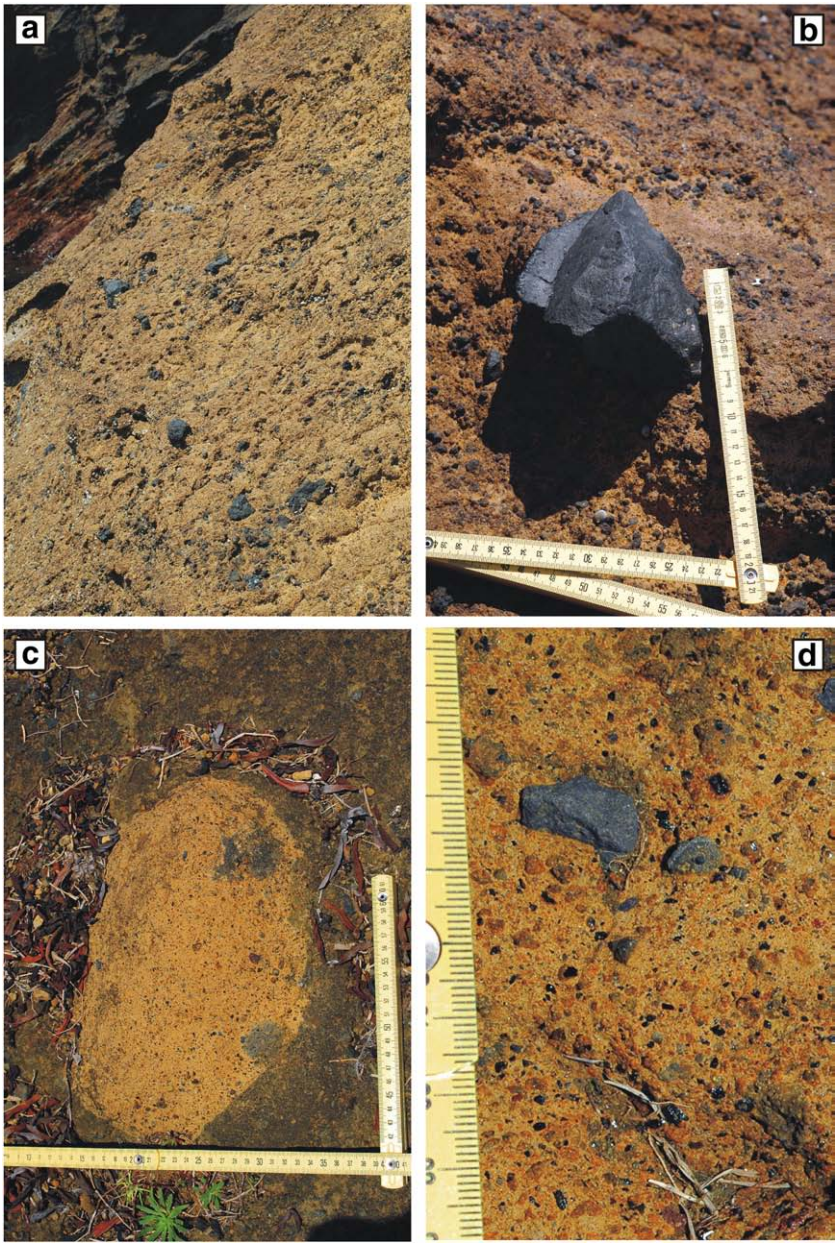

Fig. 9. Lithic bomb types in the tuff cone. Small lava fragments are widespread along some layers located at the bottom of the depositional sequence (9a). They are angular, grey-coloured and poorly weathered, as they probably belong to an older lava flow (9b). Round tuff intraclasts (max length: 55 cm) are commonly found in the products erupted during the latest stages of activity (9c). These are heavily palagonitized and zeolite-pervaded, highly cohesive and with a brittle behaviour and contain large "loose" crystals of pyroxene and olivine, small vesicular lapilli, oxidized scoria and angular fragments of a grey, poorly weathered lava flow (9d).

constituting the basement (with fragile behaviour), along a radial pattern. The whole of the freshly deposited tephra initially reacted to syn-eruptive failures of the basement showing a plastic behaviour, with slumps and tephra remobilization. Since palagonitization increased the resistance of the bulk deposit, the response to each further basement failure was a brittle behaviour and this was evidenced by the upward propagation of the radially-arranged fractures (Fig. 7a).

Many of these fractures are extensional and show an inconsistent statistical distribution in the rose diagram, both due to the total lack of measurements in the missing sectors of the cone and the progressive vent migration along the direction of the intruding dyke. The strike-slip component in these radially-arranged fractures is expressed mainly by their direction, (i.e. from N30° to N60° westwards) which is oblique to the direction of the extension (N115°W) (e.g. Jackson et al. 1992; Dowden et al. 1997; Groppelli and Tibaldi 1999; Parfitt and Peacock 2001).

Tangentially-arranged fractures are present mainly in the northern outcrop and in the small islets, and they commonly show a normal component. These are thought to testify to different post-eruptive collapses of the basement but they may also be produced by the differential loading and compaction of the deposits. Also, the two lava flows that are around the cone were intersected by these fractures and appear to have experienced extensive collapses along the whole extent of their front, especially where the lava flows surround the south-western part of the cone. In particular, close to the south-western tip of the cone, several arcuate fractures on the lava flows clearly evidence a partial collapse of the front side of the flow.

The faults discovered in the tuff cone are important as regards the displacement of the outcrop. Ring faults similar to those of other tuff cones (e.g. Sohn and Chough, 1992; Sohn and Park, 2005) were not observed. The major NW–SE trending fault caused only minor morphological changes in the main rock body.

11.4. Palagonitization and consolidation

Palagonitization can be almost contemporaneous to tuff deposition and characterizes nearly all basaltic hydromagmatic geological formations (e.g. Capelas and Capelinhos tuff cones in Azores - Solgevik et al., 2007; Cole et al., 2001; Sinker Butte Volcano in USA, Brand and White, 2007). Palagonitization is an extremely rapid process, as demonstrated by some pyroclastic sequences erupted only 50 years ago at Capelinhos volcano (Faial Island) that are already highly palagonitized and zeolitised. This sideromelane transformation induces high secondary resistance in the tuff (cohesion), thus changing stress response of the bulk tuff from pseudo-plastic to pseudo-brittle behaviour. As a consequence, the bulk of the tuff can resist isotropic stress for a long time, but its response to oriented stress will be an immediate failure, followed by the formation of fractures. Consolidation is attained through the slow and progressive expulsion of trapped fluid, particle re-arrangements and compaction. Freshly deposited tephra, produced by water-magma interaction, is commonly water-saturated, which enhances its consolidation. Due to the presence of patches of already palagonitized tuff and/or heterogeneous material both in constitution and size, this process is not homogeneous in tuff cones/rings and can trigger small differential failures of the deposits, together with the formation of small syn-eruptive and post-eruptive mud flows and intra-crater post-eruptive landslides. All these phenomena notably affected the existing morphology, resulting in the general smoothing of the edges, crater enlargements and local flank failures. In São Roque, consolidation and basement failures began immediately after the deposition of the volcanic tuff and are probably still occurring, as evidenced by the presence of fresh unfilled fractures.

12. Conclusions

Comparative field studies carried out on other tuff cones coeval to São Roque (i.e. Ilhéu de Vila Franca, in the São Miguel Island and Monte da Guia in the Island of Faial) showed breaches that follow the trend of the intruding dyke, but the cones are, nevertheless, still well preserved, indicating that besides the characteristics of the eruption and the resulting deposits, a different mechanism operates at São Roque to promote the destruction of the cone and produce its present structure.

Despite the palagonitization and zeolitisation, that indurate the pyroclastic deposits soon after their deposition, and the emplacement of at least two lava flows around the cone, São Roque has been progressively dismantled and, furthermore, post-eruptive debris-falls, rock-falls and faulting events continue to produce significant morphological changes up to recent times.

The present morphology of the São Roque tuff cone results from the concurrence of several processes, involving volcanism (a low-volume hydromagmatic eruption whose vents progressively migrated along the direction of the dyke intrusion), tectonics (syn-and post-eruptive fractures and faults) and structural behaviour of basement (basement failure). The destruction of the eastern and southern sectors of the cone is certainly related with its exposure to sea erosion but also dependent on eruptive/depositional factors and/or on deformation/displacement occurring in the basement, as well as the tectonic setting.

The main consequence of the basement rupture is the development of the observed radially-arranged and tangentially-arranged fractures which produced a network of weakness planes in the cone that led to a significant acceleration of its destruction. Also the action of NNW–SSE and NW–SE trending normal faults and of a WNW–ESE strike slip fault, probably played important roles determining the present structure of the cone and the destruction of the missing sectors.

Acknowledgements

The authors wish to thank C. Goulart of the Centro de Vulcanologia e Avaliação de Riscos Geológicos, for her assistance in the solution of all the problems related to the GIS database, and M. Neri of the Istituto Nazionale di Geofisica e Vulcanologia - Catania, Italy, for his useful suggestions regarding the discussion on the tectonics of the São Roque tuff cone. Thanks are also extended to R.J. Brown and Y.K. Sohn for their accurate and detailed editing, which has significantly improved the quality of this paper.

References

Bonatti, E., 1965. Palagonite, hyaloclastites and alteration of volcanic glass in the ocean. Bull. Volcanol. 28 (1), 257–269.
Booth, B., Walker, G.P.L., Croasdale, R., 1978. A quantitative study of five thousand years of volcanism on São Miguel, Azores. Philos. Trans. R. Soc. Lond. 228A, 271–319.
Brand, B.D., White, C.M., 2007. Origin and stratigraphy of phreatomagmatic deposits at the Pleistocene Sinker Butte Volcano, Western Snake River Plain, Idaho. J. Volcanol. Geotherm. Res. 160, 319–339.
Branney, M.J., Kokelaar, P., 2002. Pyroclastic density currents and the sedimentation of ignimbrites. Geological Society of London Memoirs, vol. 27, p. 150 pp.
Camus, G., Boivin, P., Goër de Herve, A., Gourgaud, A., Kieffer, G., Mergoil, J., Vincent, P.M., 1981. Le Capelinhos (Faial, Açores) vingt ans après son éruption: le modèle éruptiv «surtseyen» et des anneaux de tufs hyaloclastiques. Bull. Volcanol. 44, 31–42.
Cannat, M., Briais, A., Deplus, C., Escartín, J., Georgen, J., Lin, J., Mercouriev, S., Meyzen, C., Muller, M., Pouliquen, G., Rabain, A., da Silva, P., 1999. Mid-Atlantic Ridge–Azores hotspot interactions: along-axis migration of a hotspot-derived event of enhanced magmatism 10 to 4 Ma ago. Earth Planet. Sci. Lett. 173, 257–269.
Carey, S.N., 1991. Transport and deposition of tephra by pyroclastic flows and surges. In: Fisher, R.V., Smith, G.A. (Eds.), Sedimentation in volcanic setting. Society of Economic Paleontologists and Mineralogists, Special publications, pp. 39–57.
Cas, R.A.F., Wright, J.V., 1987. Volcanic Successions: Modern and Ancient. Allen and Unwin, London. 528 pp.
Chaves, F.A., 1915. Erupções submarinas nos Açores. Açoreana 5 (4), 312–361.
Chough, S.K., Sohn, Y.K., 1990. Depositional mechanics and sequences of base surges, Songaksan tuff ring, Cheju Island, Korea. Sedimentology 37, 1115–1135.
Cole, P.D., Scarpati, C., 1993. A facies interpretation of the eruption and emplacement mechanism of the upper part of the Neapolitan Yellow Tuff, Campi Flegrei, southern Italy. Bull. Volcanol. 55, 311–326.
Cole, P.D., Guest, J.E., Duncan, A.M., Pacheco, J.M., 2001. Capelinhos 1957–1958, Faial, Azores: deposits formed by an emergent surtseyan eruption. Bull. Volcanol. 63, 204–220.
Corazzato, C., Tibaldi, A., 2006. Fracture control on type, morphology and distribution of parasitic volcanic cones: an example from Mt. Etna, Italy. J. Volcanol. Geotherm. Res. 158, 177–194.
Delcamp, A., van Wyk de Vries, B., James, M.R., in press. The influence of edifice slope and substrata on volcano spreading. J. Volcanol. Geotherm. Res., doi: 10.1016/j.jvolgeores.2008.07.014.
Dellino, P., La Volpe, L., 1995. Fragmentation versus transportation mechanisms in the pyroclastic sequence of Monte Pilato — Rocche Rosse (Lipari, Italy). J. Volcanol. Geotherm. Res. 64, 211–232.
Dellino, P., La Volpe, L., 2000. Structures and grain size distribution in surge deposits as a tool for modelling the dynamics of dilute pyroclastic density currents at La Fossa di Vulcano (Aeolian Islands, Italy). J. Volcanol. Geotherm. Res. 96, 57–78.
Dellino, P., Isaia, R., La Volpe, L., Orsi, G., 2001. Statistical analysis of textural data from complex pyroclastic sequences: implications for fragmentation processes of the Agnano–Monte Spina tephra (4.1 ka), Campi Flegrei, southern Italy. Bull. Volcanol. 63, 443–461.
Dellino, P., Isaia, R., La Volpe, L., Orsi, G., 2004. Interaction between particles transported by fallout and surge in the deposits of the Agnano–Monte Spina eruption (Campi Flegrei, Southern Italy). J. Volcanol. Geotherm. Res. 133, 193–210.
Dowden, J.M., Murray, J., Kapadia, P., 1997. Changes in the stress regime and displacement field in the interior of Mount Etna deduced from surface observations. Tectonophysics 269, 299–315.
Engvik, A.K., Bertram, A., Kalthoff, J.F., Stöckhert, B., Austrheim, H., Elvevold, S., 2005. Magma-driven hydraulic fracturing and infiltration of fluids into the damaged host rock, an example from Dronning Maud Land, Antarctica. J. Struct. Geol. 27 (27), 839–854.
Ferreira, T., 2000. Caracterização da activitade vulcânica da ilha de São Miguel (Açores): vulcanismo basáltico recente e zonas de desgaseificação. Avaliação de riscos. Ph.D Thesis, University of Azores, Ponta Delgada, 248 pp.
Fisher, R.V., Schmincke, H.U., 1984. Pyroclastic rocks. Springer-Verlag, New York. 472 pp.
Fisher, R.V., Waters, A.C., 1970. Base surge bedforms in Maar Volcanoes. Am. J. Sci. 268, 157–180.
Fisher, R.V., Heiken, G., Hulen, J.B., 1997. Volcanoes: Crucibles of Change. Princeton Univ. Press, Princeton, New Jersey.
Fiske, R.S., Cashman, K.V., Shibata, A., Watanabe, K., 1998. Tephra dispersal from Myojinsho, Japan, during its shallow submarine eruption of 1952–1953. Bull. Volcanol. 59, 262–275.
Gente, P., Dyment, J., Maia, M., Goslin, J., 2003. Interaction between the Mid-Atlantic Ridge and the Azores hot spot during the last 85 Myr: Emplacement and rifting of the hot spot-derived plateaus. Geochem. Geophys. Geosyst. 4 (10), 8514–8537.
Groppelli, G., Tibaldi, A., 1999. Control of rock rheology of deformation style and slip-rate along the active Pernicana fault, Mt. Etna, Italy. Tectonophysics 305, 521–537.
Gudmundsson, A., Loetveit, I.F., 2005. Dyke emplacement in a layered and faulted rift zone. J. Volcanol. Geotherm. Res. 144, 311–327.

Gudmundsson, A., Marinoni, L.B., Marti, J., 1999. Injection and arrest of dykes: implications for volcanic hazards. J. Volcanol. Geotherm. Res. 88, 1–13.
Houghton, B.F., Hackett, W.R., 1984. Strombolian and phreatomagmatic deposits of Ohakune craters, Ruapehu, New Zealand: a complex interaction between external water and rising basaltic magma. J. Volcanol. Geotherm. Res. 21 (3-4), 207–231.
Houghton, B.F., Schmincke, H.U., 1986. Mixed deposits of simultaneous strombolian and phreatomagmatic volcanism: Rothenberg volcano, east Eifel volcanic field. J. Volcanol. Geotherm. Res. 30 (1-2), 117–130.
Houghton, B.F., Wilson, C.J.N., Smith, I.E.M., 1999. Shallow-seated controls on styles of explosive basaltic volcanism: a case study from New Zealand. J. Volcanol. Geotherm. Res. 91 (1), 97–120.
Jackson, M.D., Endo, E.T., Delaney, P.T., Arnadottir, T., Rubin, A.M., 1992. Ground ruptures of the 1974 and 1983 Kaoiki earthquakes, Mauna Loa Volcano, Hawaii. J. Geophys. Res. 97, 8775–8796.
Jiménez-Munt, I., Fernàndez, M., Torne, M., Bird, P., 2001. The transition from linear to diffuse plate boundary in the Azores–Gibraltar region; results from a thin-sheet model. Earth Planet. Sci. Lett. 192, 175–189.
Johnson, C.L., Wijbrans, J.R., Constable, C.G., Gee, J., Staudigel, H., Tauxec, L., Forjaz, V.H., Salgueiro, M., 1998. $^{40}Ar/^{39}Ar$ ages and paleomagnetism of São Miguel lavas, Azores. Earth Planet. Sci. Lett. 160, 637–649.
Kokelaar, P., 1986. Magma–water interactions in subaqueous and emergent basaltic volcanism. Bull. Volcanol. 48, 275–289.
Lanzafame, G., Neri, M., Acocella, V., Billi, A., Funiciello, R., Giordano, G., 2003. Structural features of the July–August 2001 Mount Etna eruption: evidence for a complex magma supply system. J. Geol. Soc. Lond. 160, 531–544.
Machado, F., 1959. Submarine pits of the Azores plateau. Bull. Volcanol. 21, 109–116.
Machado, F., Parsons, W.H., Richards, A.F., Mulford, J.W., 1962. Capelinhos eruption of Fayal Volcano, Azores. J. Geophys. Res. 67, 3519–3529.
Machado, F., Lemos, R., 1998. Sobre uma possivel erupção submarina no Banco D. João de Castro em 1997. Açoreana 8, 559–564.
Madeira, J., Ribeiro, A., 1990. Geodynamic models for the Azores triple junction. A contribution from tectonics. Tectonophysics 184, 405–415.
Mastin, L.G., Christiansen, R.L., Thornber, C., Lowenstern, J., Beeson, M., 2004. What makes hydromagmatic eruptions violent? Some insights from the Keanakāko'i Ash, Kīlauea Volcano, Hawai'i. J. Volcanol. Geotherm. Res. 137, 15–31.
Moore, J.G., Nakamura, K., Alcaraz, A., 1966. The 1965 eruption of Taal volcano. Science 151, 955–960.
Moore, J.G., 1967. Base surge in recent volcanic eruptions. Bull. Volcanol. 30, 337–363.
Németh, K., Cronin, S.J., 2007. Syn- and post-eruptive erosion, gully formation, and morphological evolution of a tephra ring in a tropical climate erupted in 1913 in West Ambrym, Vanuatu. Geomorphology 86, 115–130.
Parfitt, E.A., Peacock, D.C.P., 2001. Faulting in the South Flank of Kilauea Volcano, Hawaii. J. Volcanol. Geotherm. Res. 106, 265–284.
Peacock, M.A., 1926. The petrology of Iceland, Part l, the basic tuffs. Commun. - R. Soc. Edinb. Transac. 55, 53–76.
Schmincke, H.U., 2004. Volcanism. Springer Verlag, Berlin.
Searle, R., 1980. Tectonic pattern of the Azores spreading centre and triple junction. Earth Planet. Sci. Lett. 51, 415–434.
Sigurdsson, H., Fisher, R.V., 1987. The 1982 eruption of El Chichon volcano, Mexico (3): physical properties of pyroclastic surges. Bull. Volcanol. 49, 467–488.
Snyder, D.C., Widom, E., Pietruszka, A.J., Carlson, R.W., Schmincke, H.U., 2007. Time scales of formation of zoned magma chambers: U-series disequilibria in the Fogo A and 1563 A.D. trachyte deposits, São Miguel, Azores. Chem. Geol. 239 (1), 138–155.
Sohn, Y.K., Chough, S.K., 1989. Depositional processes of the Suwolbong tuff ring, Cheju Island (Korea). Sedimentology 36, 837–855.
Sohn, Y.K., Chough, S.K., 1992. The Ilchulbong tuff cone, Cheju Island, South Korea: depositional processes and evolution of an emergent, Surtseyan-type tuff cone. Sedimentology 39, 523–544.
Sohn, Y.K., Chough, S.K., 1993. The Udo tuff cone, Cheju Island, South Korea: transformation of pyroclastic fall into debris fall and grain flow on a steep volcanic cone slope. Sedimentology 40, 769–786.
Sohn, Y.K., 1996. Hydrovolcanic processes forming basaltic tuff rings and cones on Jeju Island, Korea. Geol. Soc. Am. Bull. 108, 1199–1211.
Sohn, Y.K., Park, K.H., 2005. Composite Tuff ring/cone complexes in Jeju Island, Korea: possible consequences of substrate collapse and vent migration. J. Volcanol. Geotherm. Res. 141, 157–175.
Solgevik, H., Mattsson, H.B., Hermelin, O., 2007. Growth of an emergent tuff cone: fragmentation and depositional processes recorded in the Capelas tuff cone, São Miguel, Azores. J. Volcanol. Geotherm. Res. 159 (1), 246–266.
Taylor, P.W., Ewart, A., 1997. The Tofua Volcanic Arc, Tonga, SW Pacific: a review of historic volcanic activity. Aust. Volc. Invest. Occ. Rpt. 97/01, 1–58.
Thorarinsson, S., Einarsson, T., Sigvaldason, G., Elísson, G., 1964. The submarine eruption off the Vestmann Islands 1963–1964. Bull. Volcanol. 27, 435–445.
Thorarinsson, S., 1967. Surtsey, the New Island in the North Atlantic. Viking Press, New York.
Thorseth, I.H., Furnes, H., Tumyr, O., 1991. A textural and chemical study of Icelandic palagonite of varied composition and its bearing on the mechanism of the glass-palagonite transformation. Geochim. Cosmochim. Acta 55 (3), 731–749.
Thouret, J.-C., 1999. Volcanic geomorphology — an overview. Earth Sci. Rev. 47, 95–131.
Valentine, G.A., Fisher, R.V., 2000. Pyroclastic surges and blasts. In: Sigurdsson, H., Houghton, B.F., McNutt, S.R., Rymer, H., Stix, J. (Eds.), Encyclopedia of Volcanoes. Academic Press, pp. 571–580.
Vaughan, R.G., Abrams, M.J., Hook, S.J., Pieri, D.C., 2007. Satellite observations of new volcanic island in Tonga. Eos, Trans. Amer. Geophys. Union 88, 37–41.
Vespermann, D., Schmincke, H.U., 2000. Scoria cones and tuff rings. In: Sigurdsson, H., Houghton, B., McNutt, S.R., Rymer, H., Stix, J. (Eds.), Encyclopedia of Volcanoes. Academic Press, San Diego, pp. 683–694.
Vogt, P.R., Jung, W.Y., 2004. The Terceira Rift as hyper-slow, hotspot-dominated oblique spreading axis: a comparison with other slow-spreading plate boundaries. Earth Planet. Sci. Lett. 218, 77–90.
Walker, J.D., Croasdale, R., 1971. Two Plinian-type eruptions in the Azores. J. Geol. Soc. Lond. 127 (1), 17–55.
Washington, H.S., 1909. The submarine eruptions of 1831 and 1891 near Pantelleria. Am. J. Sci. 27, 130–150.
White, J.D.L., 1996. Impure coolants and interaction dynamics of phreatomagmatic eruptions. J. Volcanol. Geotherm. Res. 74 (3), 155–170.
White, J.D.L., Houghton, B., 2000. Surtseyan and related phreatomagmatic eruptions. In: Sigurdsson, H., Houghton, B.F., McNutt, S.R., Rymer, H., Stix, J. (Eds.), Encyclopedia of Volcanoes. Academic Press, San Diego, pp. 495–511.
Wilson, C.J.N., Hildreth, W., 1998. Hybrid fall deposits in the Bishop Tuff, California: a novel pyroclastic depositional mechanism. Geology 26, 7–10.
Wohletz, K.H., Sheridan, M.F., 1979. A model of pyroclastic surge. Geol. Soc. Am. Sp. Pap. 180, 177–194.
Wohletz, K.H., Sheridan, M.F., 1983. Hydrovolcanic eruptions: II. Evolution of basaltic tuff rings and tuff cones. Am. J. Sci. 283, 385–413.
Zanon, V., 2005. Geology and volcanology of San Venanzo volcanic field (Umbria, Central Italy). Geol. Mag. 142 (6), 683–698.
Zanon, V., Neri, M., Pecora, E., in press. Interpretation of data from the monitoring thermal camera: the case of Stromboli volcano (Aeolian Islands, Italy). Geol. Mag.
Zhou, Z., Fyfe, W.S., 1989. Palagonitization of basaltic glass from DSDP Site 335, Leg 37: textures, chemical composition, and mechanism of formation. Am. Mineral. 74, 1045–1053.